Humidity Responsive Reflection Grating Made by Ultrafast Nanoimprinting of a Hydrogel Thin Film

Stefan Cesnik, Alberto Perrotta, Alessandro Cian, Massimo Tormen, Alexander Bergmann,* and Anna Maria Coclite*

The response time of state-of-the-art humidity sensors is ≈8 s. A faster tracking of humidity change is especially required for health care devices. This research is focused on the direct nanostructuring of a humidity-sensitive polymer thin film and it is combined with an optical read-out method. The goal is to improve the response time by changing the surface-to-volume ratio of the thin film and to test a different measurement method compared to state-of-the-art sensors. Large and homogeneous nanostructured areas are fabricated by nanoimprint lithography on poly(2-hydroxyethyl methacrylate) thin films. Those thin films are made by initiated chemical vapor deposition (iCVD). To the author's knowledge, this is the first time nanoimprint lithography is applied on iCVD polymer thin films. With the imprinting process, a diffraction grating is developed in the visible wavelength regime. The optical and physicochemical behavior of the nanostructures is modeled with multi-physic simulations. After successful modeling and fabrication a first proof of concept shows that humidity dependency by using an optical detection of the first diffraction order peak is observable. The response time of the structured thin film results to be at least three times faster compared to commercial sensors.

1. Introduction

The measurement of humidity is an important parameter in a wide field of applications ranging from industry to the human body. Over the past years, many different devices for humidity sensing were fabricated. Standard devices for measuring humidity are so-called hygrometers, which quantify the amount of water vapor in the air. Psychrometers measure the temperature difference between a dry and wet bulb, while dew point hygrometers use the optical detection of the condensation on a chilled surface. Also gravimetric methods for the determination of the amount of water are used, but those methods are very time consuming and therefore often used in calibration processes.[1] State of the art humidity sensors basically work by measuring the change of the capacity or impedance of a polymer or metal oxide film layer.[2,3]

On the other side, functional polymers also gained a high amount of interest during the last years, especially as materials for sensing devices.

As new materials and applications emerge, the employment of nanoscale surface topographies has steadily grown and novel techniques able to process them are continuously developed. Nanoimprinting lithography (NIL) configures itself as a very affordable and simple method to transfer micro and nanostructures onto a malleable material. In its basic form, that is, thermal NIL or T-NIL, a rigid surface-structured stamp is mechanically pressed into a deformable material (typically a polymer) and heat is applied with temperatures above the glass transition temperature of the material. During the imprinting process, the material flows into the cavities of the stamp. After cooling and removal of the stamp, the structure pattern is transferred to the material. The simplicity of the process has certainly allowed its widespread adoption in research. Moreover, the possibility of the parallel

S. Cesnik, A. Bergmann
Institute of Electrical Measurements and Sensor Systems
Graz University of Technology
Graz 8010, Austria
E-mail: alexander.bergmann@tugraz.at

A. Perrotta
Italian National Research Council-Institute of Nanotechnology
(CNR-NANOTEC)
via Orabona 4, Bari 70126, Italy

A. Cian
Center for Materials and Microsystems
Fondazione Bruno Kessler
FBK, Via Sommarive 18, Trento I-38123, Italy

M. Tormen
ThunderNIL S.r.l.
Area Science Park, Trieste 34149, Italy

A. M. Coclite
Institute of Solid State Physics, NAWI Graz
Graz University of Technology
Petersgasse 16, Graz 8010, Austria
E-mail: anna.coclite@tugraz.at

ADVANCED
SCIENCE NEWS
www.advancedsciencenews.com

[M] **acro-**
olecular
Rapid Communications
www.mrc-journal.de

processing of large-area substrates with high-throughput and high-resolution has extended its attractiveness to industries, especially invested in optoelectronic devices, nanofluidics, and diverse biological applications.[4] However, in the standard T-NIL, both heating and cooling steps are energy and time consuming, and the overall process can reach up to tens of minutes. Ultrafast T-NIL is an advanced NIL method that allows the processability of the technique to be applied in the range of µs.[5,6] It relies on the use of a stamp with an integrated heater buried below the surface. By µs-short electric pulses, the stamp is heated to higher temperatures, localized to the sole surface without deforming/damaging the bulk material.[7] This results in a process with high heating/cooling rates and reduces dramatically the overall process timing.

The present paper focuses on the direct nanostructuring of polymer thin films with hundreds of nanometer thickness. These thin films are deposited on substrates with a special technique, the so-called initiated chemical vapor deposition (iCVD).[8] Currently, initiated chemical vapor deposition is well understood and it offers a large variation of usable materials.[9] Especially, the study and application of hydrogels got attention in the past years. Hydrogels are polymeric networks with the feature to change their initial thickness by orders of magnitudes when environmental conditions such as temperature, relative humidity or pH-value change.[10] Hydrogel thin films can be made with iCVD as well.[11]

Although the deposition of hydrogel thin films with iCVD is well-known so far, the direct structuring of iCVD-made polymers was limitedly reported. A previous example is known with capillary force lithography.[12] Nevertheless, the most common techniques to nanostructure hydrogels are using templates made of anode aluminum oxide (AAO)[13,14] or nanosphere lithography.[15–17] The fabrication of nanoporous micro-structures[18] with iCVD was also achieved. In this work we used poly(2-hydroxyethyl methacrylate), which is a well-known RH-responsive hydrogel. The response to humidity of poly(2-hydroxyethyl methacrylate) was previously studied.[19] Additionally, previous works of our group[20] showed that the combination of poly(2-hydroxyethyl methacrylate) hydrogels with interference based detection methods could be promising for future sensor applications. While the previous work[20] described an interference based measurement setup from planar thin films, the current work focuses on the nanostructuring of such thin films, while still using an optical detection method for the humidity response. The work of Buchberger[20] pointed out that optical based read out methods showed an almost three times faster response times compared to commercial state-of-the-art humidity sensors.[3] Electrical humidity sensors with fast response time have also been reported.[21] However, optical humidity sensors can be promising devices in fuel cells and for the determination of gas humidity in pipelines or explosive environments. Also the fabrication of AAO templates with nanosphere lithography was successfully shown.[22] A general way to structure polymer films was reported with direct structuring methods with femtosecond lasers[23] or electron beam lithography (e-beam).[24,25] Additional methods of structuring polymers can be found in [26–29]. Some works successfully created hydrogel nanostructures using AAO (anode aluminum oxide) templates[14] or colloidal lithography.[30] A summary of lithog-

raphy based methods[27,31] can be found in the literature, too. However, the pre-described techniques are often expensive or the nanostructures sometimes irregularly arranged or rather they just covered small areas of the substrate. Most of the time also post treatment is required. Additionally, direct structuring with e-beam is a very time consuming process. Since hydrogels are polymers which have a so-called glass transition temperature, we found a way to successfully imprint nanostructures onto the topside of iCVD-made thin film surfaces with a thermal lithography.

In the present work the authors goal is to demonstrate the application of ultrafast NIL to structure the surface of iCVD polymers with periodic nanosized patterns. The design and physical effect of the nanostructures was successfully modeled with multi-physic simulations by the commercial available software COMSOL. We also performed a first proof of concept experiment to detect the humidity correlation of the nanostructures with a laser based read out method. Furthermore, the future goal is to improve the response time by trying to increase the surface-to-volume ratio of the hydrogel thin film. Imprinting a line array on top of the polymer thin film was advantageous, because of following reasons: first, hydrogels offer great optical properties in the visible wavelength regime and second, diffraction gratings are well known and can be described by the grating equation

$$m \cdot \lambda = g \cdot \sin(\Theta_m) \tag{1}$$

with Θ_m being the angle of m-order diffraction peaks, the different wavelengths λ and the grating constant g. Additionally, Equation (1) only includes information of the position of the peaks but not about the intensity distribution.

For the sensing mechanism we choose an optical based measurement method, contrary to the state-of-the-art impedance measurement based technique. The great optical properties of iCVD grown thin films derived from their smoothness were combined with their fast responsive behavior to environmental changes and finally to achieve highly faster response times than conventional humidity sensors. Additionally, optical methods offer the advantage to have the measurement-detector system locally separated from each other which could open new fields for unconventional applications as well. Furthermore, iCVD thin films can be composed of different polymers, making them responsive to humidity,[19] temperature,[32,33] or pH-value.[34]

2. Results and Discussion

2.1. Nanoimprint Lithography on Thin Film Polymers

First of all the thickness of the iCVD deposited planar thin film was measured with an ellipsometer and after application of a Cauchy fit model (see Equation (S1), Supporting Information) its thickness resulted to be (528.8 ± 0.1) nm.

The fabrication process of nanostructured thin films was done in cooperation with ThunderNIL srl (Area Science Park, Trieste, Italy) and is described in detail in Section 4. Our first test structure was produced with a line array stamp to print a large-area diffraction grating on top of the hydrogel thin film layer. Gratings with two different grating constants $g = 500$ nm and 800 nm were imprinted. The dimensions of the imprinting stamps are shown
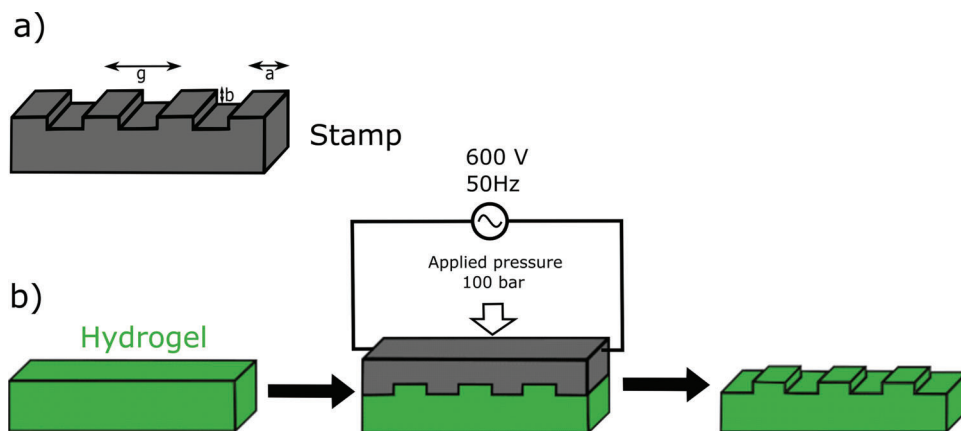
Figure 1. Schematic sketch of the nanoimprinting process with the stamp (gray) and the hydrogel (green) with a= linewidth, b= depth, and g= grating constant.
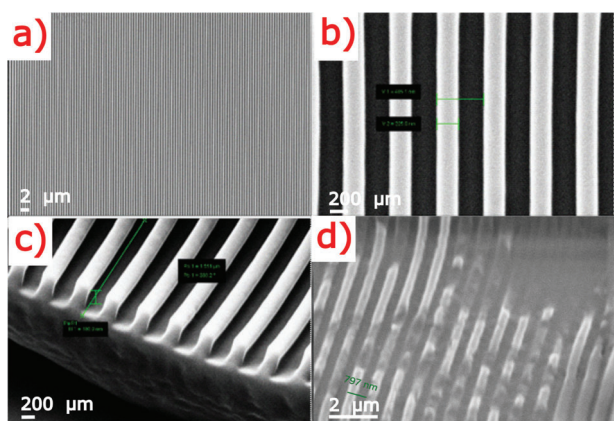
Figure 2. Overview of the hydrogel thin film after nanoimprinting process. a) Overview of the 500 nm grating. b,c) The imprinted line array in detail. d) The 800 nm grating.

in **Figure 1**a and with $a = 250$ nm, $b = 200$ nm, $g = 500$ nm, and $a = 400$ nm, $b = 200$ nm, $g = 800$ nm respectively. During the imprinting procedure the stamp is heated above the glass transition temperature T_g of the polymer ($T_{stamp} > T_g$) to print the structure on the thin film surface as schematically drawn in Figure 1b.

The characterization of the nanostructures was done with a scanning electron microscope as presented in **Figure 2**: Figure 2a shows an overview of the sample after the imprinting process. Figure 2b is a magnification of a) to compare the structure and stamp dimensions. Figure 2c shows a cross section, where the height of the nanostructure can be measured. Additionally, the original hydrogel planar thin film can be seen below the nanostructure grating. Figure 2d shows again an overview of the sample with $g = 800$ nm grating constant. Defects are shown in Figure S2a,b, damaged areas can be simply overprinted, without damaging the sensitive hydrogel thin film layer around. From the authors knowledge the combination of ultrafast nanoimprinting lithography on iCVD polymer thin films was done for the first time.
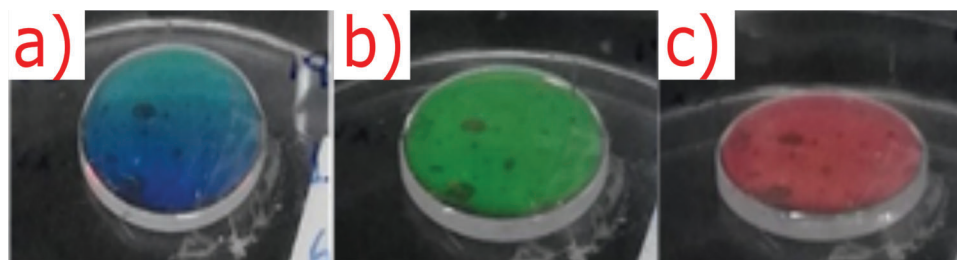
For our example we choose a specific structure-to-wavelength ratio for excitation of diffraction modes regarding to Equation

(S2). The defects from Figure S2a,b, have different origins: The defects in Figure S2a, were present prior the imprinting process. Probably they are due to some dust particles or handling of the thin film with tweezers after the iCVD process. Contrary, the defects from Figure S2b, seem to appear after removing the stamp. However, the defects did not affect the sensor performance: the patterned area was so large, that the defects could be easily avoided during the measurements.

As already aforementioned NIL offers the great advantage to fabricate large areas (cm regime) of nanostructures. Since our structure contains periodic arrangements of lines in 1D, also the diffracted light occurs under preferred orientation angles of the sample. Therefore, the diffraction grating effect can even be observed by eye over the whole sample as demonstrated in **Figure 3**: here we can see snapshots of the sapphire samples (17.25 mm diameter) with the nanostructured hydrogel on top, taken with a camera for different viewing angles. As expected from Equation (1) the wavelengths a) blue, b) green, and c) red are separately observed for different viewing angles. On the sample surface some thin film defects can be seen but they do not lead to problems during or after the fabrication process. Furthermore, the whole sample can be nanostructured within one imprinting process. The possibility of overprinting thin film defects as indicated in Figure 2d points out the robustness of the structured layer which is, inter alia, a main criteria for later sensor applications. The fast NIL technique from ThunderNIL could be particularly suitable for mass productions of such thin film samples in the future.

2.2. Multiphysic Modeling

Before testing the obtained patterned in a real sensor, we modeled the physical phenomenon with the software COMSOL. For our current project we utilized two modules, namely the optical wave module with the hygroscopic swelling module. From our knowledge the coupling of the optical and the linear elastic model was done for the first time. p(HEMA) hydrogels are known to absorb water when exposed to humidity and swell by increasing their size up to two or three times the original one. We used COMSOL simulations to see how the swelling would

**ADVANCED
SCIENCE NEWS**

www.advancedsciencenews.com

**[M]acro-
molecular
Rapid Communications**

www.mrc-journal.de

Figure 3. Overview of the imprinted samples for different viewing angles. Diffraction of a) blue, b) green, and c) red light. The indicative angle of view resulted to be 22°, 41°, and 52°, respectively.
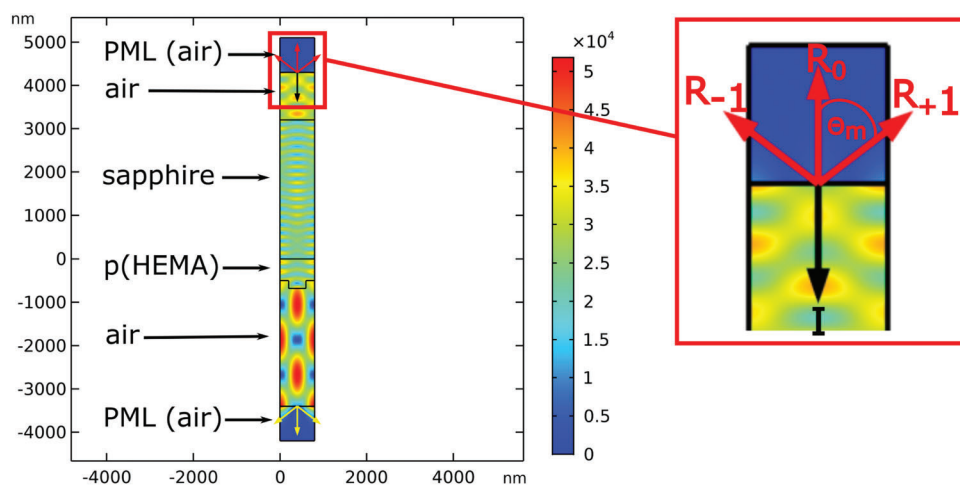
Figure 4. Result of the optical simulation for 0° incident angle, $g = 800$ nm grating constant and without swelling of the hydrogel. The color bar indicates the strength of the electromagnetic field. The arrows label the k-vectors for the reflected (red) and incident (black) light.

proceed over the grating. First, we simulated the interaction with light of the unswollen structure. This result of the optical simulation is shown in **Figure 4**: Here the normalized electromagnetic field was calculated for the unswollen unit cell with $g = 800$ nm grating constant, since the swelling measurements in Section 2.3 were also taken only at this grating constant. Similar to the experimental conditions we calculated the reflected and transmitted electromagnetic waves from top to bottom side. In Figure 4 the transmitted part of the light is stronger than the reflected one. We can also see that the waves are absorbed on top and bottom side, which is expected due to the perfectly matched layer boundaries.
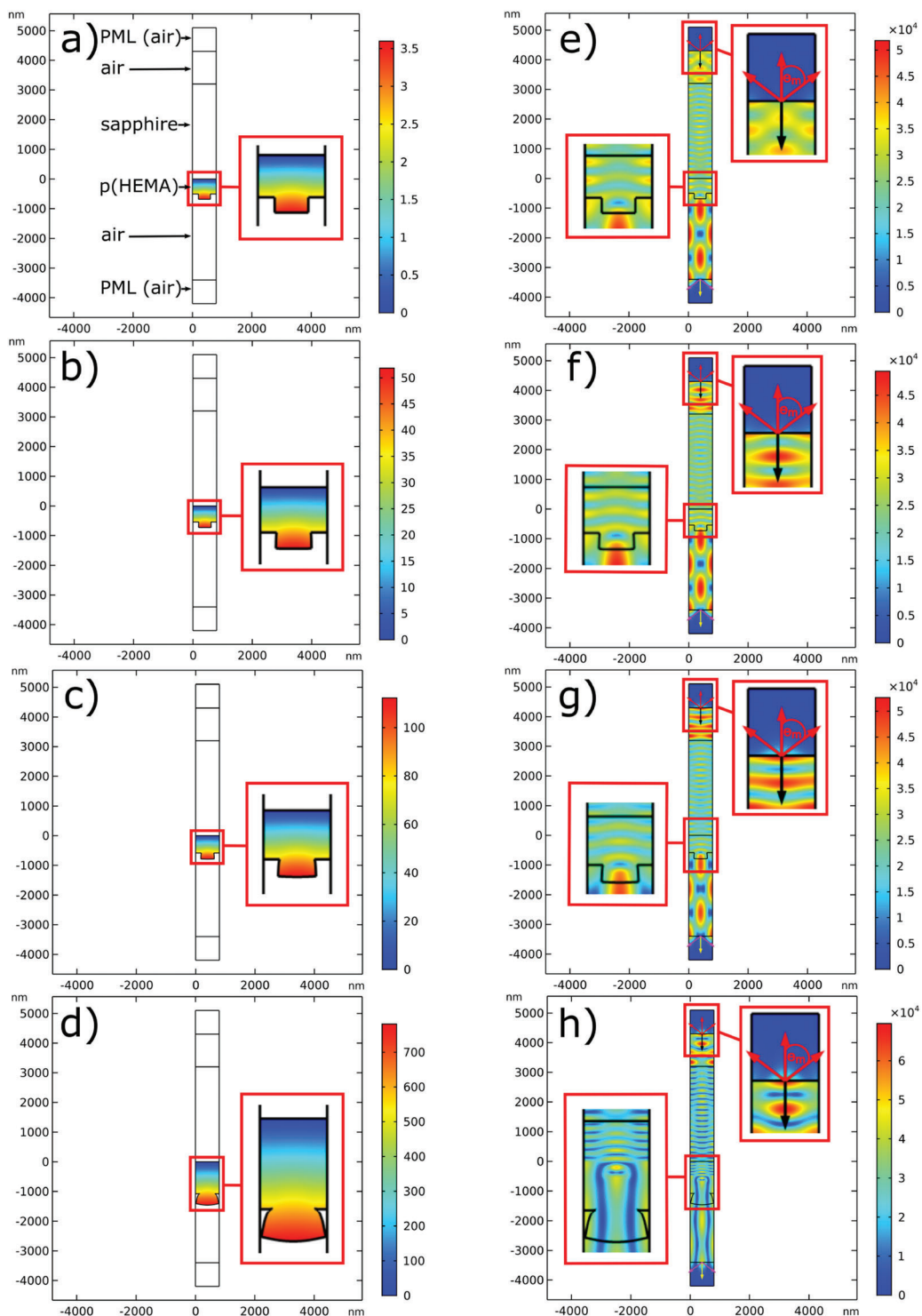
Furthermore, COMSOL enables the option to plot the k-vectors as arrows of incoming (black), transmitted (blue), and reflected (red) waves. Since, we are were mainly interested in the reflected signal, this region was zoomed out in Figure 4. The labeled red arrows R_0, R_{-1}, and R_{+1} represent the orders of reflection for $m = 0$ (direct reflected beam), $m = -1$, and $m = +1$, respectively. The resulting value $\Theta_m = 52°$ agrees very well with the theoretical calculation from Equation (1).

Finally, we also included the swelling behavior of the hydrogel from known experimental data (see Figure S3, Supporting Information) into the simulation model and thus combined the optical and swelling solutions. The results are presented in **Figure 5** in the following way: (a–d) represent the swelling simulation of the hydrogel region for humidity values of 3%, 50%, 73%, and 95%, respectively. For better visualiza-

tion the swelling regions are magnified. As expected from the experimental measurements (see Figure S3, Supporting Information) the swelling begins to increase at high humidity levels. The scale shows the calculated displacement field for hygroscopic swelling.

Additionally, the plots (e–h) in Figure 5 highlight the combined results of swelling and optical simulation for 0° incident angle. Here, also the k-vectors of the reflected (red) and incident light (black) were plotted. For better visualization the areas of interest are zoomed out. Contrary to figures (a–d) the colored scale in those figures indicates the normalized electromagnetic field and the swelling is indicated by the change of the geometric frame. Furthermore, the diffraction angle Θ_m (see Equation (1)) figures (e– h) remains constant in. That can be explained by grating equation (1), which does not include any information about the grating height.

At this point, it is also important to mention that COMSOL is a FEM based software, which uses different types and geometries of meshes to solve physical equations. Therefore, the size of the structure is a limiting factor for the computation time. Also in our example, we had to do a trade-off regarding the substrate height, because it has a thickness in the millimeter range, contrary to the nanometer size structures. Therefore, it is not possible to use the exact geometry of the substrate (2 mm height) for the simulation. However, the height of the substrate does not influence the position of the diffraction peaks for 0° incident angle.

ADVANCED
SCIENCE NEWS

www.advancedsciencenews.com

{M} acro-
molecular
Rapid Communications

www.mrc-journal.de

Figure 5. Result swelling solution combined with the optical solutions. a–d) The result of the swelling hydrogel for 3% RH, 50% RH, 73% RH, and 95% RH. The values were taken from experimental swelling curves. The color bar shows the swelling in terms displacement of the structure. g–f) The swelling (same values as (a–d)) combined with the optical simulation for 0° incident angle. The red arrows highlight the k-vectors of the reflected electromagnet wave, the black arrow of the incident wave. The color bar shows the strength of the electromagnetic field.

ADVANCED
SCIENCE NEWS
www.advancedsciencenews.com

[M] acro-
molecular
Rapid Communications
www.mrc-journal.de

In the hygroscopic swelling area in Figure 8 we used "roller boundary conditions" for the planar film and free boundary conditions for the nanostructure swelling for the following reasons: We consider the swelling in the vertical direction being much more dominant than the one in the longitudinal direction due to the presence of the substrate. This behavior is modeled with the roller boundary conditions in COMSOL. Contrary to planar films, which are directly adsorbed on the substrate, the nanostructure grating is located on top of them and hence not bound on any surface. Thus, the swelling of the nanostructure will most likely not be limited in any direction, which was the reason of setting free boundary conditions for them.

The multiphysic simulation highlighted that the position of the diffraction peaks does not change for different swollen geometries as shown in Figure 4. Here, it must be mentioned, that the swelling is in general very weak for low humidity concentrations as demonstrated in the swelling curves in Figure S3, Supporting Information. However, the diffraction angle stayed constant till 95% RH (see Figure 4e)). We interpret based on the simulation results that the grating constant is not going to change effectively, if the displacement of the structure is equal in both horizontal directions.

A great advantage of the actual COMSOL model is the compact development, which occurs from the chosen symmetries and boundary conditions. Therefore, the transition to different grating constants can be adjusted very fast and additionally, other periodic structures should also be easy to include.

2.3. Humidity Correlation

After successful fabrication of the nanostructures we looked for an effect to detect the dependency of the new structured thin film for different humidity levels. Since the new imprinted structure (see Figure 2) is a diffraction grating we took a monochromatic light source and measured if correlation of humidity changes and the first order diffraction peak is detectable. First, we used a simple setup as shown in Figure 9 and noticed that the position of the diffraction peaks agrees well with the theoretical value from Equation (1) and the simulated angle. Furthermore, the diffraction peaks for m={+1,-1} were, as expected, observed in reflection and transmission due to the transparent substrate. However, in our setup and for the first proof of concept we only focused on the reflected part. Regarding to Equation (1) we first thought that swelling is going to lead to increasing grating constants and therefore in a shift of the diffraction peak. However, in our first experiments the diffraction peak did not shift on the observation screen. This result agrees well with the COMSOL simulation from Figure 5e–f.

We prepared samples with $g = 500$ and 800 nm grating constant, because diffraction are detectable for both configurations. The humidity measurements are shown with $g = 800$ nm grating, because it turned out that the nanostructures with diffraction grating constant $g = 500$ nm vanished for humidity values above 70%. Since p(HEMA) has increased swelling at high humidity (see Figure S3, Supporting Information) the nanostructures stick together and collapsed. As consequence we tried to reduce the probability that at high swelling the nanostructure would touch and stick by increasing the spacing between them. Therefore, we
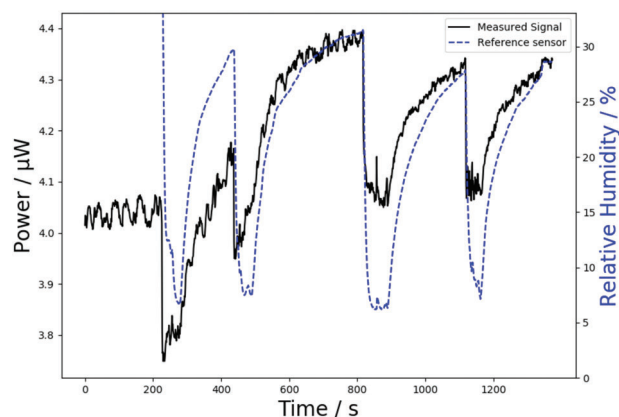
Figure 6. Measurement of the first order diffraction peak intensity (black curve) for changing humidity (blue curve).
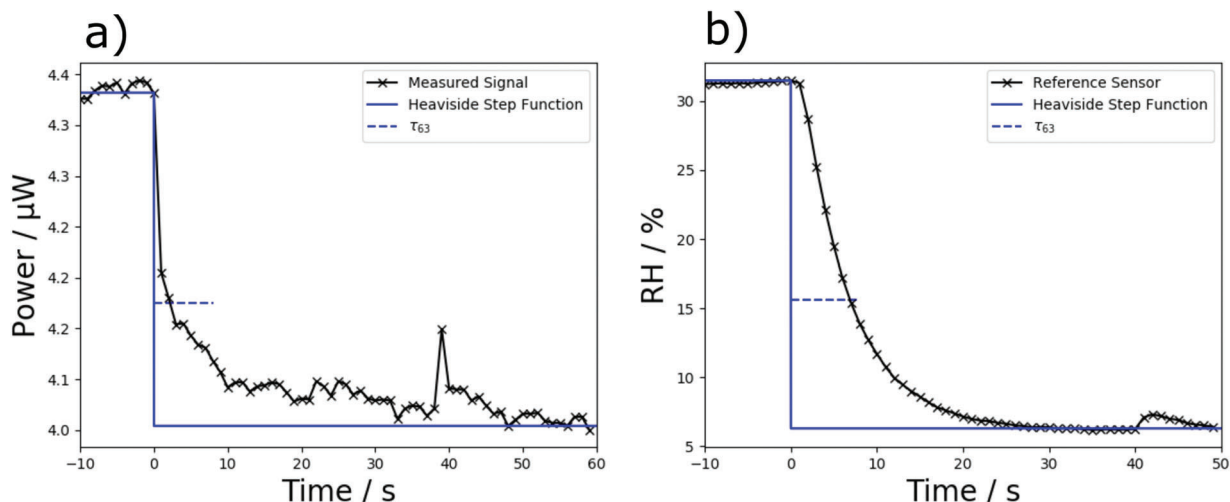
continued our measurement with humidity ranging from 5% RH to ambient (30% RH) and 800 nm grating constant and the drawn measurement setup from Figure 9 in Section 4.

Figure 6 shows the measured reflected laser intensity (black line) of the first order diffraction peak for varying relative humidity levels (reference sensor, blue dashed line). In Figure 6 clear correlations between measured laser power and humidity are observed. A drop of the humidity resulted in a drop of the laser signal and vice versa. Furthermore, the position of the diffraction peak did not move during the swelling / deswelling process of the hydrogel (see Figure S4, Supporting Information). Finally, the response time was measured for the nanostructured hydrogel with optical readout and the reference sensor at $t = 800$ s (Figure 6) and resulted to be (2 ± 1) s. and (7 ± 1) s, respectively. For humidity sensors the response time is defined by the time when 63% of the signal is reached. The response time was calculated by fitting a Heaviside step function as shown in **Figure 7**a,b into the measured signal. The response time of the reference sensor agrees well with its data sheet.

Additionally, the power seems to derive for the first cycles and it stabilizes after the second cycle which can be explained that in the current study relative thick thin film with around 500 nm were deposited, which may need a few cycles to get mechanically stabilized. While the maximum power very nicely follows the RH variation, the minimum seems to increase steadily. This trend we also noticed with the ellipsometric measurements in previous works.[35,36] It seems like the hydrogel retains a minimum amount of water and it rearranges. Furthermore, the behavior of the refractive index of a planar p(HEMA) thin film for different RH levels is reported in Figure S1, Supporting Information.

Regarding Equation (1) the peak position depends on the grating constant for fixed wavelengths, but especially, for low humidity values the swelling is very low, as visible from the ellipsometric measurement (see Figure S3, Supporting Information) and also in the simulation.

Since we did the NIL experiments for the first time, we did not know how the good the stability of the nanostructures would be, considering that the hydrogel is quite soft thin film.. We noticed that the actual nanostructures do not vanish (even after weeks) while storing them under normal ambient conditions.

**ADVANCED
SCIENCE NEWS**

www.advancedsciencenews.com

[M]acro-
molecular
Rapid Communications

www.mrc-journal.de

Figure 7. Response times for a) optical method and b) reference sensor. The blue line fits a Heavyside step function into the signals.

Since a lot of sensors primary operate by impedance measurements, we think that optical read out methods could be promising in the future. Especially, hydrogel thin films combined with optical based read out methods stands out with response times being three times faster than commercial impedance measurement based sensor systems.

The actual limitation for the high relative humidity regime could be investigated by adding more cross-linker during the deposition process to decrease the swelling. Finally, we also want to mention that the shown sensor system is still in an early stadium, but the first results seem very promising for detailed future studies.

3. Conclusion

In summary we demonstrated the fabrication of nanostructures using ultrafast nanoimprint lithography on iCVD made hydrogels. The unique combination of iCVD polymers and ultrafast NIL has proven a direct method to produce large-area surface-nanostructured thin film polymers (Figure 3). The well-established plethora of polymer chemistries achieved with iCVD can then be combined with ultrafast NIL to explore different sensors and nano-devices. Specifically, adopting a hydrogel, the nanostructured surface was applied as a humidity sensor. It demonstrated to achieve measurable improvements compared to commercially available impedance sensors and serves as a valuable proof-of-concept for further implementations and device improvements. In detail we also showed that the dimensions of structure fit very well with the geometry of the stamp (Figure 2). The grating effect can be observed for our configuration by eye (Figure 3) and, as well, with a monochromatic laser source for the visible wavelength regime.

In the simulation part we successfully showed that our diffraction grating can be modeled with a FEM based software (COMSOL) by using a unit cell (Figure 4). This optimized development leads to low computation times and furthermore, parameters as grating constant, laser wavelength, or material parameters can be changed very quickly. We also combined two different models, namely the optical wave module and the hygroscopic swelling module (Figure 5). The next steps are going to be the validation of the swelling behavior and sensor effect with a detailed experimental study.

The stability of the imprinted grating is given while stored under ambient conditions but the nanostructures vanish for relative humidity levels above 70%. Furthermore, we also showed a possible sensor effect by measuring the reflected intensity of the first diffraction order, which correlated with changing relative humidity (Figure 7). Additionally, the response time was faster than previous planar nonstructured thin films studies from our group. Finally, we want to mention that the sensor system is a proof of concept. The first tests seem to be promising to study the sensing behavior of the structured hydrogel for various applications.

4. Experimental Section

Modeling of the Nanostructure: The simulation was performed with COMSOL 5.4 on a PC workstation with 16 core processor and 128 GB memory. COMSOL is a commercial FEM software with the opportunity to work with multi-physic coupling during one simulation. The goal of the simulations was to support the experimental design of nanostructures and furthermore, to implement the optical and material properties of the structured hydrogel thin film. In COMSOL it can be very useful to work with symmetries to reduce the computational time. For this specific case, a simple unit cell was able to be made, because the structure acts as diffraction grating, which can be simply described as a periodic arrangement of lines with different depths. The wave optics module was utilized to simulate the optical properties of the structure. In this work, the optical structure effect was successfully combined with the swelling properties of the hydrogel.

Since, the NIL imprinted patterns were periodic line arrays, the whole structures acted as a diffraction grating for the visible wavelength regime. Therefore the setup can be implemented in COMSOL very effectively by creating a unit cell with periodic boundary conditions, similar to the real samples. The utilized materials were developed equal to the experimental situation and are shown in **Figure 8**: Starting from topside the unit cell contains two air regions, followed by sapphire (substrate), p(HEMA) (hydrogel), and again two air regions. Figure 8 also includes different types of boundary conditions (colored lines), which will be described in the next subsection.

Wave Optics Module: The hatched areas in Figure 8 are so-called "perfectly matched layer" (PML) in COMSOL. These perfectly matched

www.advancedsciencenews.com

{M} acro-molecular
Rapid Communications
www.mrc-journal.de
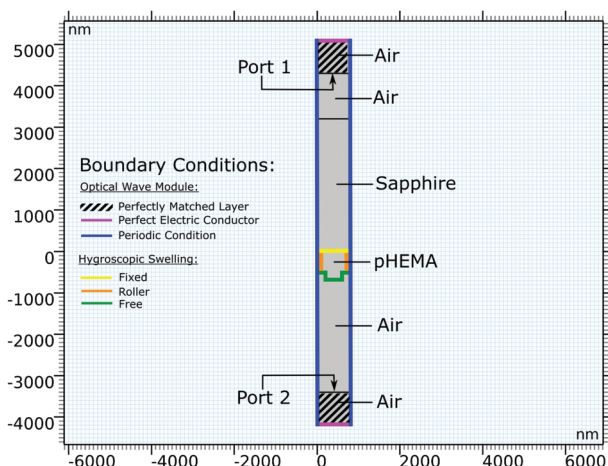
Figure 8. Detailed sketch of the developed unit cell with the boundary conditions for the optical wave module and the hygroscopic swelling module.

Figure 9. Experimental setup for the observation of the position of the first order diffraction peak and for measuring humidity dependency.

layers were domains to ensure that no undesirable electromagnetic waves were reflected back into the ports. The blue boundaries were periodic boundary conditions and the magenta colored lines were perfect electric conductor boundaries. Finally, for the propagation of electromagnetic waves and excitation port (Port 1) and a transmission port (Port 2) were needed. Additionally, Port 1 received simultaneously the reflected part of the light. The optical simulations were performed with the perfect structure-to-wavelength ratio (see Equation (S2), Supporting Information) of the diffraction grating which was, of course, never accomplished in the experimental situation. The wavelength of the incident electromagnetic wave at Port 1 was set to 635 nm, similar to the laser in the experiment.

Hygroscopic Swelling: The swelling was simulated from experimental curves recorded by in-house ellipsometry (see Supporting Information). In Figure 8 the orange lines were rolling boundary conditions. They prevented the hydrogel to swell in the horizontal direction. For the nanostructure part free boundary conditions, indicated as green, were set. Finally, fixed boundary conditions (yellow) were chosen at the interface between substrate and hydrogel.

Fabrication of Thin Films: The thin film deposition was done in a custom build reactor which was already described.[37] Polymers of 2-hydroxyethyl methacrylate (Sigma Aldrich) were deposited on Si-wafers and sapphire substrates (Edmund optics, diameter = 17.25 mm). The Si-wafers were used to measure the thickness of the thin films by laser interference in situ and for further FTIR spectra from the thin film. Sapphire windows served as templates for humidity measurements. As initiator for the polymerization tert-butyl peroxide (Sigma Aldrich) was used. The monomer HEMA was heated up to 75 °C. The working pressure during the thin film deposition was held at 400 mTorr. The substrate and filament temperatures were 35 °C and 300 °C, respectively.

Fabrication of Nanostructures: The nanoimprinting was achieved through an ultrafast NIL with the collaboration of ThunderNIL srl (Area Science Park, Trieste, Italy). The NIL process is schematically shown in Figure 2 with the stamp (gray) and the hydrogel thin film (green). The ultrafast NIL was achieved through the use of nanostructured stamps with an integrated heater. A full description of the principle of work is reported in ref. [5]. The integrated heater consisted of a heavily n-type doped silicon layer buried below the nanostructured surface of the stamp. The stamp was contacted and heated by Joule effect, by applying current pulses flowing in the conductive layer of 105 μs at 50 Hz repetition rate. The temperatures achieved by Joule effect during the μs pulse are up to 600 °C and were limited to the stamp surface, delivering ultrafast printing of nanometric sized structures.[6] Due to the short time range of the process, only few hundreds of nanometers of the surface were affected by the imprinting process while the bulk of the material was not altered, as schematically reported in Figure 2. The average pressure applied on the backside of the
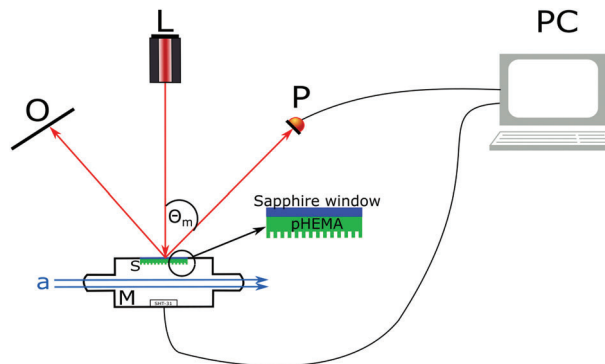
wafer was 100 bar and the voltage applied was 600 V. The pulse was delivered on stamps with a resistance of 1.6 ohm. A sketch of the stamp adopted in this work is drawn in Figure 1. The nanostructure consisted of line gratings with three different configurations available: 1) $g = 800$ nm and $a = 400$ nm; 2) $g = 500$ nm and $a = 250$ nm; 3) $g = 300$ nm and $a = 150$ nm. The height $b = 200$ nm was equal for both stamps. The stamps were fabricated by a combination of laser interference lithography and thermal NIL and the ultrafast NIL at ThunderNIL srl.

Thin Film Characterization: Spectra of the deposited p(HEMA) thin film were recorded with a FTIR spectrometer and are shown in Figure S5b, Supporting Information. The peak at 1700 cm^{-1} was well known and indicates the C=O stretching. Peaks at 2900 cm^{-1} and 3400 cm^{-1} show CH$_3$— and O—H -stretching, respectively.

The thickness of the thin film was measured with an ellipsometer (Woolam, M2000 VASE) and after application of a Cauchy fit model its thickness resulted to be (528.8 ± 0.1) nm.

Humidity Measurement Setup: The setup was built to measure the power of the first reflected diffraction pattern. **Figure 9** sketches the setup for humidity measurements. A laser (L, Thorlabs, 635 nm center wavelength, 4.5 mW output power) was directed at the sapphire substrate (S) with the nanostructured hydrogel on its backside. For reflection measurements the laser penetrated through the sapphire window, hence the substrate had to be transparent for the visible wavelength regime. The diffraction grating effect ensured to detect the first order diffraction pattern. The intensity of one diffraction pattern was measured with a powermeter (P, Thorlabs). A red filter in front the powermeter reduced ambient light, while an observation screen (O, Figure S4, Supporting Information) detected the position of the second diffraction pattern. The custom 3D printed measurement chamber (M) was flooded with compressed synthetic air (a) and a reference sensor (Sensirion SHT-31) measured the change of relative humidity simultaneously. Additionally, the measurement chamber was mounted on a rotation stage (Thorlabs). Powermeter as well as reference sensor were connected to a PC and read out with their specific softwares Thorlabs Optical Power Monitor and USB RS485 Sensor Viewer, respectively. The measurement chamber was printed with a Formlabs 3D printer using black resin to reduce the transmitted light within the chamber.

Supporting Information

Supporting Information is available from the Wiley Online Library or from the author.

Acknowledgements

Conflict of Interest

The authors declare no conflict of interest.

Data Availability Statement

The data that support the findings of this study are available from the corresponding author upon reasonable request.

Keywords

humidity sensors, hydrogel thin films, nanoimprint lithography

[1] C.-Y. Lee, G.-B. Lee, *Sens. Lett.* **2005**, *3*, 1.
[2] H. Farahani, R. Wagiran, M. N. Hamidon, *Sensors* **2014**, *14*, 7881.
[3] F. Weller, D. Keller, S. Wettstein, M. Graf, *Proceedings* **2018**, *2*, 13.
[4] Y. Chen, *Appl Phys. A* **2015**, *121*, 451.
[5] M. Tormen, R. Malureanu, R. H. Pedersen, L. Lorenzen, K. H. Rasmussen, C. J. Lüscher, A. Kristensen, O. Hansen, *Microelectron. Eng.* **2008**, *85*, 1229.
[6] M. Tormen, E. Sovernigo, A. Pozzato, M. Pianigiani, M. Tormen, *Microelectron. Eng.* **2015**, *141*, 21.
[7] M. Pianigiani, R. Kirchner, E. Sovernigo, A. Pozzato, M. Tormen, H. Schift, *Microelectron. Eng.* **2016**, *155*, 85.
[8] W. E. Tenhaeff, K. K. Gleason, *Adv. Funct. Mater.* **2008**, *18*, 979.
[9] S. J. Yu, K. Pak, M. J. Kwak, M. Joo, B. J. Kim, M. S. Oh, J. Baek, H. Park, G. Choi, D. H. Kim, J. Choi, Y. Choi, J. Shin, H. Moon, E. Lee, S. G. Im, *Adv. Eng. Mater.* **2018**, *20*, 1700622.
[10] S. Dwivedi, et al., *Int J Pharm Biol Arch* **2011**, *2.6*, 1588.
[11] K. Chan, K. K. Gleason, *Langmuir* **2005**, *21*, 8930.
[12] S. G. Im, K. W. Bong, B.-S. Kim, S. H. Baxamusa, P. T. Hammond, P. S. Doyle, K. K. Gleason, *J. Am. Chem. Soc.* **2008**, *130*, 14424.
[13] L. Wen, R. Xu, Y. Mi, Y. Lei, *Nat. Nanotechnol.* **2017**, *12*, 244.
[14] G. O. Ince, G. Demirel, K. K. Gleason, M. C. Demirel, *Soft Matter* **2010**, *6*, 1635.
[15] C. L. Cheung, R. J. Nikolić, C. E. Reinhardt, T. F. Wang, *Nanotechnology* **2006**, *17*, 1339.
[16] P. Colson, C. Henrist, R. Cloots, *J. Nanomaterials* **2013**, *2013*, 948510.
[17] C. L. Haynes, R. P. Van Duyne, *J. Phys. Chem. B* **2001**, *105*, 5599.
[18] H. Sojoudi, S. Kim, H. Zhao, R. K. Annavarapu, D. Mariappan, A. J. Hart, G. H. McKinley, K. K. Gleason, *ACS Appl. Mater. Interfaces* **2017**, *9*, 43287.
[19] K. Unger, R. Resel, A. M. Coclite, *Macromol. Chem. Phys.* **2016**, *217*, 2372.
[20] A. Buchberger, S. Peterka, A. M. Coclite, A. Bergmann, *Sensors* **2019**, *19*, 5.
[21] S. Taccola, F. Greco, A. Zucca, C. Innocenti, C. de Julián Fernández, G. Campo, C. Sangregorio, B. Mazzolai, V. Mattoli, *ACS Appl. Mater. Interfaces* **2013**, *5*, 6324.
[22] M. Krupinski, M. Perzanowski, A. Maximenko, Y. Zabila, M. Marszałek, *Nanotechnology* **2017**, *28*, 194003.
[23] F. Korte, J. Serbin, J. Koch, A. Egbert, C. Fallnich, A. Ostendorf, B. N. Chichkov, *Appl Phys. A* **2003**, *77*, 229.
[24] R. Zandi Shafagh, A. Vastesson, W. Guo, W. van der Wijngaart, T. Haraldsson, *ACS Nano* **2018**, *12*, 9940.
[25] W. Yue, Z. Wang, Y. Yang, L. Chen, A. Syed, K. Wong, X. Wang, *J. Micromech. Microeng.* **2012**, *22*, 125007.
[26] S. Nejati, K. K. S. Lau, *Nano Lett.* **2011**, *11*, 419.
[27] C. Acikgoz, M. A. Hempenius, J. Huskens, G. J. Vancso, *Eur. Polym. J.* **2011**, *47*, 2033.
[28] D. Li, J. Huang, R. B. Kaner, *Acc. Chem. Res.* **2009**, *42*, 135.
[29] H. D. Tran, D. Li, R. B. Kaner, *Adv. Mater.* **2009**, *21*, 1487.
[30] N. J. Trujillo, S. Baxamusa, K. K. Gleason, *Thin Solid Films* **2009**, *517*, 3615.
[31] Y. Ofir, I. W. Moran, C. Subramani, K. R. Carter, V. M. Rotello, *Adv. Mater.* **2010**, *22*, 3608.
[32] O. Werzer, S. Tumphart, R. Keimel, P. Christian, A. M. Coclite, *Soft Matter* **2019**, *15*, 1853.
[33] F. Muralter, A. M. Coclite, O. Werzer, *J. Phys. Chem. C* **2019**, *123*, 24165.
[34] Z. Zhang, L. Chen, C. Zhao, Y. Bai, M. Deng, H. Shan, X. Zhuang, X. Chen, X. Jing, *Polymer* **2011**, *52*, 676.
[35] F. Muralter, A. Perrotta, A. M. Coclite, *Macromolecules* **2018**, *51*, 9692.
[36] P. Salzmann, A. Perrotta, A. M. Coclite, *ACS Appl. Mater. Interfaces* **2018**, *10*, 6636.
[37] C. Ranacher, R. Resel, P. Moni, B. Cermenek, V. Hacker, A. M. Coclite, *Macromolecules* **2015**, *48*, 6177.